Anomalous diffusion and power-law relaxation of the time averaged mean squared displacement in worm-like micellar solutions

Anomalous diffusion and power-law relaxation of the time averaged mean squared displacement in worm-like micellar solutions

Jae-Hyung Jeon[1]**, Natascha Leijnse**[2]**, Lene B Oddershede**[2] **and Ralf Metzler**[1,3,4]

[1] Department of Physics, Tampere University of Technology, 33101 Tampere, Finland
[2] Niels Bohr Institute, University of Copenhagen, 2100 København Ø, Denmark
[3] Institute for Physics and Astronomy, University of Potsdam, 14476 Potsdam-Golm, Germany
E-mail: rmetzler@uni-potsdam.de

Abstract. We report the results of single tracer particle tracking by optical tweezers and video microscopy in micellar solutions. From careful analysis in terms of different stochastic models, we show that the polystyrene tracer beads of size 0.52–2.5 μm after short-time normal diffusion turn over to perform anomalous diffusion of the form $\langle \mathbf{r}^2(t) \rangle \simeq t^\alpha$ with $\alpha \approx 0.3$. This free anomalous diffusion is ergodic and consistent with a description in terms of the generalized Langevin equation with a power-law memory kernel. With optical tweezers tracking, we unveil a power-law relaxation over several decades in time to the thermal plateau value under the confinement of the harmonic tweezer potential, as predicted previously (*Phys. Rev.* E **85** 021147 (2012)). After the subdiffusive motion in the millisecond range, the motion becomes faster and turns either back to normal Brownian diffusion or to even faster superdiffusion, depending on the size of the tracer beads.

[4] Author to whom any correspondence should be addressed.

IOP Institute of Physics Φ DEUTSCHE PHYSIKALISCHE GESELLSCHAFT

Contents

1. Introduction

Following Robert Brown's original studies of microscopic particles ejected by pollen grains [1], it was Jean Perrin at the Sorbonne in Paris who developed advanced protocols for extensive single particle tracking [2]. Perrin's experiments relied on relatively short trajectories such that he used *ensemble averages* over many individual particle displacements to compute the diffusion constant of the tracer particles. A few years later Ivar Nordlund at the University of Uppsala came up with the idea of following a single mercury droplet over long times through projection of the particle motion onto a moving film [3]. Nordlund's method allowed him to calculate the diffusion coefficient via the *time average* of an individual droplet's trajectory, without the need to average over many, not completely identical particles. Today, the tracking of single tracer particles or even single, labelled molecules has become a standard tool to probe the dynamics of tracers in living biological cells or other microscopic systems [4, 5].

Single particle tracking has become the tool of choice to investigate the effect of *molecular crowding*, the superdense environment present in the cytoplasm of living biological cells. Molecular crowding may reach a volume occupation of up to 40% by biomacromolecules, and thus cause major changes of the motion of large biopolymers and artificial tracers as well as the function of enzymes [6–8]. Indeed, the observed motion of freely diffusing molecules and tracers in living cells exhibits significant deviations from the linear time dependence of the mean squared displacement (MSD) $\langle \mathbf{r}^2(t) \rangle \simeq t$ characteristic of Brownian motion. Instead, *anomalous diffusion* [9–11] of the form $\langle \mathbf{r}^2(t) \rangle \simeq t^\alpha$ with $0 < \alpha < 1$ has been widely reported. Thus, fluorescently labelled messenger RNA molecules in *Escherichia coli* (*E. coli*) bacteria cells subdiffuse with $\alpha \approx 0.7$ even when altering the physiological conditions or disrupting the bacterium's cytoskeletal internal structure [12]. Similar findings, with different values of α, were reported for the motion of DNA loci in *E. coli* [13], lipid granules [14, 15], viruses [16] and for chromosomal end parts (telomeres) in eukaryotic nuclei [17]. Anomalous diffusion in the cytoplasm of living cells was also reported from studies using fluorescence correlation spectroscopy [18, 19]. In artificially crowded control environments anomalous diffusion is consistently observed [18, 20–22]. Finally, the crowding in cellular membranes also gives rise to anomalous diffusion phenomena [23, 24], as also observed in extensive simulation studies [25–28].

Here we report new results from single particle tracking of polystyrene microbeads in micellar solutions. Worm-like micelles are long cylindrical objects self-assembled by cationic surfactants [29]. In a semi-dilute regime above a critical concentration c^*, worm-like micelles form a transient polymer network, where segments of micelle polymers constantly break and recombine in several ways depending on the micellar concentration. Microrheology studies have shown that under this condition the worm-like micelles behave like a typical viscoelastic material [29–31]. Combining results from tracking with an optical tweezers setup and a more conventional video microscopy tracking assay, we show that in the millisecond range even at a low micellar concentration of 1% weight the tracers exhibit anomalous diffusion consistent with motion in a viscoelastic environment as described by the generalized Langevin equation with a power-law kernel. The anomalous diffusion exponent characterizing the bead motion is $\alpha \approx 0.3$. Moreover, we demonstrate that under confinement as exerted on the tracer beads by the Hookean restoring force of the optical tweezer, we observe a power-law relaxation to the equilibrium plateau value, as opposed to the conventional exponential relaxation. This observation is consistent with recent analytical and numerical results [32]. Finally, we show that at long times the majority of beads move normally ($\alpha \approx 1$). However, similar to previous experimental findings in micellar solutions [33] some larger beads also show superdiffusive motion ($\alpha > 1$).

After presenting the experimental system and a primer on theoretical models for anomalous diffusion in section 2, we report the results from the optical tweezers and video tracking experiments in section 3. Finally, in section 4 we discuss the results and draw conclusions.

2. Experimental and theoretical background

2.1. Materials and methods

2.1.1. Worm-like micelles.   Worm-like micelles were mixed according to a protocol from [34]. Cetylpyridinium chloride (CPyCl, Sigma, acts as a surfactant) and sodium salicylate (NaSal, Sigma, strongly binding counter ions) were mixed and dissolved in 0.5 M NaCl. For the micelle concentration of 1 wt% we used molar concentrations of $0.06\,\mathrm{mol\,l^{-1}}$ CPyCl, $0.03\,\mathrm{mol\,l^{-1}}$ NaSal dissolved in $0.5\,\mathrm{mol\,l^{-1}}$ NaCl in Milli-Q water. The samples were equilibrated for at least 1 day prior to measurements and stored at room temperature. All experiments were conducted at room temperature. The micelle concentration of 1 wt% implies that the solution is in the semi-dilute regime ($c > c^*$, $c^* \sim 0.3\,\mathrm{wt}\,\%$) in which micelles are entangled.

Physically, worm-like micelles are elongated self-assembled structures formed by a spontaneous aggregation of surfactant molecules (amphiphiles). Their viscoelastic properties depend on their concentration and the electrolytes in the solvent. Under the current conditions, the micelles grow into elongated tubular structures which constantly break and re-form, similar to the ongoing polymerization/depolymerization in certain polymers [29].

2.1.2. Preparation of samples.   The micelles were mixed with 0.4% of a solution of uncoated polystyrene beads (0.52, 0.96 $2.5\,\mu$m, Bangs Labs) dissolved in Millipore water. $100\,\mu$l of the final mixture was added to a clean coverslip ($24 \times 50\,\mathrm{mm}^2$, #1.5, Menzel–Gläser) bottom in between two strips of vacuum grease. In order to create a chamber, a clean coverslip ($18 \times 18\,\mathrm{mm}^2$, #1, Menzel–Gläser) was tightly pressed on top. Care was taken not to induce

air bubbles inside the micelles/bead sample. The sample sides were sealed with vacuum grease to create a closed chamber.

2.1.3. Optical tweezers tracking. The motion of beads in worm-like micellar solutions was recorded using optical tweezers tracking with photodiode detection resulting in a time resolution of 4.5×10^{-5} s. The optical trap was implemented in an inverted microscope (Leica DMIRBE) where the laser beam (Nd:YVO$_4$ (5W Spectra Physics BL106C, $\lambda = 1064$ nm, TEM$_\infty$)) was tightly focused by a water immersion objective (Leica, HCX PL APO, 63×, NA = 1.2, COR R CS). The laser light scattered by the moving beads passing the sample was collected by a condenser (Leica, P1 1.40 oil S1) and focused on the back focal plane of a quadrant photodiode (S5981, Hamamatsu). Data were acquired by a data acquisition card (NI PCI-6040E) at a sampling frequency of 22 kHz and processed by custom written LabVIEW programs (LabVIEW 2010, National Instruments). The laser power was kept relatively low (63 mW at the exit of the laser of which $\sim 65\%$, 41 mW, reached the sample) with a typical measurement time of 3 s. The temperature increase related to absorption of the laser light is expected to be well below 1 °C [35, 36]. The laser was focused on a bead (which was at least 5 μm away from any surface of the chamber) and positioned such that the bead was in the centre of the weak harmonic potential exerted by the optical trap [37]. The voltage output from the photodiode is linearly related to the small displacement of the bead with respect to the laser focus. In order to convert the voltage output from the photodiode to metric distance, knowledge about the viscosity of the medium surrounding the bead would be required. As this parameter is unknown, the MSD data for optical trapping tracking are given in arbitrary units. The three orthogonal translational directions are uncorrelated and all measurements were taken in two dimensions.

2.1.4. Single particle tracking. In order to track the motion of a bead at longer time scales than is possible by optical tweezers tracking, we imaged the beads using bright field microscopy. The microscope setup was the same as for the optical tweezers tracking but images were acquired with an AVT Pike F100B camera (Allied Vision Technologies) and SmartView (Allied Vision Technologies) acquisition software. Approximately 225 frames per second were recorded during a total measurement time of $\sim$40 s. Bead trajectories were obtained using the MOSAIK Image J single particle tracking tool [38].

2.2. Ensemble and time averaged mean squared displacements

To quantify the average diffusive behaviour of tracer particles, the conventional approach is the ensemble averaged (EA) MSD. The EA MSD is defined from the trajectories $\mathbf{r}_i(t)$ of the diffusing particles (labelled with the index i) in terms of the distance from their initial position $\mathbf{r}_i(0)$,

$$\langle \mathbf{r}^2(t) \rangle = \frac{1}{N} \sum_{i=1}^{N} (\mathbf{r}_i(t) - \mathbf{r}_i(0))^2. \tag{1}$$

Here N is the total number of measured particles. Alternatively, the diffusion of an individual particle can be quantified from the single trajectory $\mathbf{r}(t)$ via the time averaged (TA) MSD as [39, 40]

$$\overline{\delta^2(\Delta)} = \frac{1}{T - \Delta} \int_0^{T-\Delta} (\mathbf{r}(t + \Delta) - \mathbf{r}(t))^2 \, dt, \tag{2}$$

where Δ is the lag time and T is the total measurement time. Thus the TA MSD is constructed from the particle displacement during the time lag Δ accumulated over the entire trajectory. For Brownian motion both definitions are always equivalent, $\overline{\delta^2(\Delta)} = \langle \mathbf{r}^2(\Delta) \rangle$, if only the measurement time T is sufficiently long [39, 40]. More care has to be taken when we encounter anomalous diffusion. While stochastic motion of the viscoelastic type as described mathematically by fractional Brownian motion or the generalized Langevin equation with a power-law memory kernel (see below) are ergodic and self-averaging, and thus EA MSD and TA MSD are equivalent for long T [32, 41, 42], transiently non-ergodic behaviour occurs when the tracer particle engages with the confinement [32]. For anomalous diffusion of the continuous time random walk (CTRW) type involving scale-free distributions of waiting times [10, 43, 44], EA MSD and TA MSD are never equivalent. In fact, already for free motion the associated TA MSD $\overline{\delta^2(\Delta)} \simeq \Delta/T^{1-\alpha}$ scales linearly with Δ despite the underlying anomalous motion ($\langle \mathbf{r}^2(t) \rangle \simeq t^\alpha$), and shows a pronounced scatter of amplitudes [39, 40, 45–48]. The discrepancy between EA MSD and TA MSD for this type of anomalous diffusion is intimately connected to the phenomenon of weak ergodicity breaking [49–52].

For shorter time series, the TA MSD of an individual tracer may become quite erratic, in particular, for larger values of the lag time Δ approaching the overall measurement time T. The behaviour may be smoothed by calculation of the trajectory-to-trajectory average

$$\left\langle \overline{\delta^2(\Delta)} \right\rangle = \frac{1}{N} \sum_{i=1}^{N} \overline{\delta_i^2(\Delta)} \tag{3}$$

obtained from individual TA MSD $\overline{\delta_i^2(\Delta)}$. This averaging procedure is useful to estimate the scaling of the TA MSD curve from many individual TA MSD curves.

In what follows, we concentrate on one dimension of the observed two-dimensional (2D) motion for simplicity.

2.3. Anomalous diffusion under confinement

To model diffusion under the confinement exerted by the optical tweezers, we recall that to a good approximation this optical trap effects a harmonic potential on a dielectric object in its focus. The polystyrene beads thus experience the quadratic potential $U(x) = kx^2/2$ with the stiffness k, which depends on the absorption and scattering properties of the medium as well as the size and refractive index of the beads. In the experiment, the trap is initially focused on the bead corresponding to $x(0) = 0$. Recently this problem has been studied for several anomalous diffusion models in terms of the TA MSD, showing that the TA MSD exhibits different relaxation profiles depending on diffusion models, and thus the origin of the underlying diffusive process can be identified by the relaxation profile. The main results are summarized below.

2.3.1. Overdamped Brownian motion.
In regular Brownian motion under confinement in the potential $U(x)$, the EA MSD at long times approaches the saturation value $\langle x^2 \rangle_{\text{th}} = k_{\text{B}}\mathcal{T}/k$, where $k_{\text{B}}\mathcal{T}$ represents thermal energy at temperature $\mathcal{T}$. The relaxation to this stationary value occurs in the form

$$\overline{\delta^2(\Delta)} = 2\langle x^2 \rangle_{\text{th}}(1 - e^{-k\Delta/\gamma}) \tag{4}$$

except in the vicinity of $\Delta = T$ [32]. Here γ is the friction coefficient of the particle. Thus an exponential decay profile is expected for ordinary Brownian diffusion. Note the factor of 2 at equilibrium compared to the EA MSD, which is due to the definition (2) of the TA MSD [32]. In equation (4), we also assumed that the measurement time is sufficiently long (ideally, $T \to \infty$) such that the process can be assumed to be self-averaging and the single time average (4) is practically indistinguishable from that of other trajectories, $\overline{\delta_i^2(\Delta)}$.

2.3.2. Continuous time random walk. Subdiffusive CTRW is a non-ergodic anomalous diffusion model that is characterized by multiple trapping events [10, 43, 44]. The distribution of trapping times is of asymptotic power-law form $\psi(\tau) \sim \tau^{-1-\alpha}$, where $0 < \alpha < 1$, such that the resulting motion in free space becomes subdiffusive with the scaling $\langle \mathbf{r}^2(t) \rangle \sim t^\alpha$. The resulting diverging characteristic waiting time $\int_0^\infty \tau \psi(\tau) \mathrm{d}\tau$ leads to the violation of ergodicity for these processes, as there is no scale compared to which the limit of long times (large number of jumps) could be defined. In the case of subdiffusive CTRW dynamics of confined motion in the potential $U(x)$, the TA MSD of a particle starting at the flat bottom of the parabolic potential scales linearly with the lag time,

$$\left\langle \overline{\delta^2(\Delta)} \right\rangle \simeq \frac{\Delta}{T^{1-\alpha}}, \tag{5}$$

as long as Δ is sufficiently short [39, 40, 53]. Without further knowledge about the dynamics of the system, the linear scaling $\overline{\delta^2(\Delta)} \sim \Delta$ with the lag time in equation (5) would erroneously lead to the assumption that one observes normal Brownian motion. Analysis with complementary statistical tools is therefore important [15, 24, 54, 55]. Note also that in equation (5) we used the additional average (3) over many trajectories, as subdiffusive CTRW processes are no longer self-averaging and display significant fluctuations around the mean (3) [39, 42, 46]. Once the particle engages with the confinement, instead of approaching the thermal value a second power-law with exponent $1 - \alpha$ emerges [39, 40, 53],

$$\left\langle \overline{\delta^2(\Delta)} \right\rangle \simeq \left(\frac{\Delta}{T} \right)^{1-\alpha}. \tag{6}$$

Phenomen (5) and (6) were indeed observed for the anomalous motion of lipid granules inside living yeast cells [15] and in the membrane walls of human cells [56]. One can also identify CTRW-like anomalous diffusion by its ageing property: at a fixed lag time, the TA MSD decreases as $T^{\alpha-1}$ with the measurement time T, as demonstrated for the motion of protein channels in the cell wall of living human kidney cells [24]. Moreover, the effect of a time difference between the system preparation and start of the measurement was recently discussed [57].

2.3.3. Fractional Langevin equation. The fractional Langevin equation (FLE) is a generalized Langevin equation driven by power-law correlated Gaussian noise and with a power-law memory kernel [41, 58]. In free one-dimensional space the FLE reads

$$m \frac{\mathrm{d}^2 x(t)}{\mathrm{d}t^2} = -\gamma \int_0^t \mathrm{d}t' |t - t'|^{-\alpha} \frac{\mathrm{d}x}{\mathrm{d}t'} + \eta \xi(t), \tag{7}$$

where the correlated Gaussian noise $\xi(t)$ satisfies $\langle \xi(t) \rangle = 0$ and $\langle \xi(t)\xi(t') \rangle = (2-\alpha)(1-\alpha)$ $K_\alpha |t-t'|^{-\alpha}$ with $0 < \alpha < 1$ at $t \neq t'$ (where K_α is a generalized diffusion coefficient

of the dimension $[\text{cm}^2/\text{s}^\alpha]$), and its proportionality constant is chosen to be $\eta = \sqrt{\gamma k_B \mathcal{T}/[(2-\alpha)(1-\alpha)K_\alpha]}$ satisfying the fluctuation–dissipation theorem. Its solution shows that FLE motion is ballistic, $\overline{\delta^2(\Delta)} \sim \Delta^2$, below the momentum relaxation time and becomes subdiffusive, $\overline{\delta^2(\Delta)} \sim \Delta^\alpha$ $(0 < \alpha < 1)$, in the overdamped limit [41, 42]. In this limit the stochastic behaviour of FLE motion is equivalent to subdiffusive fractional Brownian motion [27, 41], where the subdiffusion is characterized by its anti-persistent motion, i.e. $\left\langle \frac{dx(t)}{dt} \frac{dx(t')}{dt'} \right\rangle \sim \alpha(\alpha-1)|t-t'|^{\alpha-2}$. It is known that the FLE-like ergodic anomalous diffusion can arise in a viscoelastic medium due to the memory effect [59, 60].

Confined FLE motion has the TA MSD [32]

$$\overline{\delta^2(\Delta)} = 2\langle x^2 \rangle_{\text{th}} \left(1 - E_\alpha \left[-\frac{k}{\gamma \Gamma(1-\alpha)} \Delta^\alpha \right] \right) \tag{8}$$

in the overdamped limit. $E_\alpha(z) = \sum_{i=0}^{\infty} z^i / \Gamma(1+\alpha i)$ is the Mittag–Leffler function and $\Gamma(z)$ is the gamma function. At short lag times we thus observe free, ergodic anomalous diffusion $\overline{\delta^2(\Delta)} \simeq \Delta^\alpha$. It can be shown that in the long-time limit the TA MSD is simplified to [32]

$$\overline{\delta^2(\Delta)} \sim 2\langle x^2 \rangle_{\text{th}} \left(1 - \frac{\gamma}{k\Delta^\alpha} \right). \tag{9}$$

Therefore, a power-law decay of the relaxation profile to the stationary plateau $\overline{\delta^2(\Delta)} \to 2\langle x^2 \rangle_{\text{th}}$ is expected for FLE-like anomalous diffusion, in contrast to the exponential relaxation (4) observed for Brownian diffusion and the power-law growth of the TA MSD (6) for CTRW.


3. Results

We first discuss the results of the optical tweezers tracking setup, which covers the time range from sub-milliseconds to seconds, before turning to video tracking in the time window from hundreds of milliseconds to some 100 seconds. These complementary techniques thus provide information on the particle motion over more than six decades in time. Moreover, we obtain valuable insight into the relaxation behaviour of the tracer in the harmonic trap of the optical tweezer.

3.1. Short-time confined motion measured by optical tweezers

The tracking data from the optical tweezers setup allows us to study the turnover from free to confined motion of individual polystyrene beads immersed in the worm-like micellar solution. Figure 1 illustrates the TA MSD curves (2) of ten individual beads of diameters $d = 0.52 \, \mu\text{m}$ (green), $0.96 \, \mu\text{m}$ (red) and $2.5 \, \mu\text{m}$ (blue) at 1 wt% concentration of worm-like micelles. In the figure the thick black lines represent the trajectory-to-trajectory average $\langle \overline{\delta^2(\Delta)} \rangle$ from ten individual TA MSD curves for each bead size. Clearly for all three groups of curves individual TA MSDs $\overline{\delta^2(\Delta)}$ nicely follow the trend given by the average behaviour. At the same time, we observe some moderate trajectory-to-trajectory amplitude scatter in each group of data. The scatter in $\overline{\delta^2}$ appears to increase with the bead size.

As we show, the immersed beads illustrate anomalous confined motion, which cannot be explained by the simple picture of a corralled Brownian particle, i.e. a Brownian particle under confinement. To see this, we note that for short lag times of the order of 0.1 ms, when the beads are not yet influenced by the restoring force of the optical tweezers, the TA MSDs exhibit the
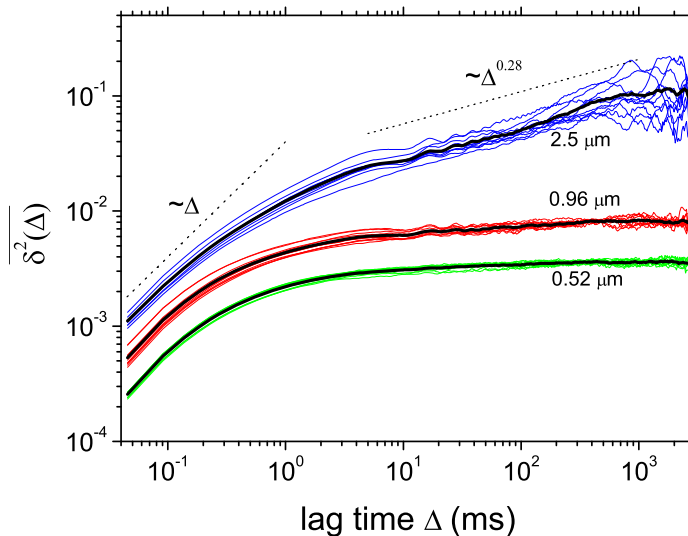
Figure 1. TA MSDs $\overline{\delta^2(\Delta)}$ for beads moving in the harmonic tweezer potential in a 1 wt% worm-like micellar solution. Initially positioned at the bottom of the harmonic potential, the beads move freely before eventually engaging with the confinement. Green: $d = 0.52\,\mu\text{m}$ beads; red: $d = 0.96\,\mu\text{m}$ beads; blue: $d = 2.5\,\mu\text{m}$ beads. In each case, $\overline{\delta^2(\Delta)}$ from ten different single trajectories are shown, while the solid black line represents their average, $\langle\overline{\delta^2(\Delta)}\rangle$. The TA MSDs for the beads of $d = 2.5\,\mu\text{m}$ size were shifted upwards for clarity. Due to lack of calibration in the optical tweezer experiments (see section 2.1.3) the ordinate is in arbitrary units, compare, however, figure 2.

linear scaling of free Brownian motion regardless of their size. Beyond this timescale, however, the relaxation dynamics of the beads becomes influenced by combined effects of the worm-like micelles and the optical trap. Even for small beads of diameters $d = 0.52$ and $0.96\,\mu\text{m}$, for which the relaxation profiles reach their saturation plateau rather quickly and thus appear similar to confined Brownian motion, the viscoelasticity of the media indeed comes into play. To show this, in figure 2, we compare the averaged relaxation curve for the $d = 0.96\,\mu\text{m}$ beads in the micellar solution to the curve for the same-sized trapped beads in pure water (the control). While the trapped beads in the control experiment rapidly approach the equilibrated state within 1 ms, surprisingly the beads in the worm-like micellar solution relax very slowly, until ~ 1 s. That is, due to the presence of 1 wt% worm-like micelles the relaxation becomes slowed-down, remarkably by at least three orders of magnitude in time. This result strongly suggests that the diffusion of the micron-sized beads in the worm-like micellar solution is, in fact, anomalous on time scales from milliseconds to seconds. This observation is confirmed by the (partially) overlapping video tracking data presented in section 3.2.

To clarify the stochastic nature of the underlying diffusive process, we quantify the relaxation behaviour based on the theoretical results summarized in section 2.3. As expected, the relaxation curve (i.e. the TA MSD) of the bead in water in figure 2 decays exponentially towards its equilibrated state, perfectly described by the form (4) for the overdamped Brownian motion in a harmonic potential. The best fit to the curve $f_{\text{ex}}(\Delta) = 2\langle x^2\rangle_{\text{th}}(1 - C_1 e^{-C_2\Delta})$ is depicted by the black solid line in figure 2. However, the exponential relaxation pattern $f_{\text{ex}}(\Delta)$ does
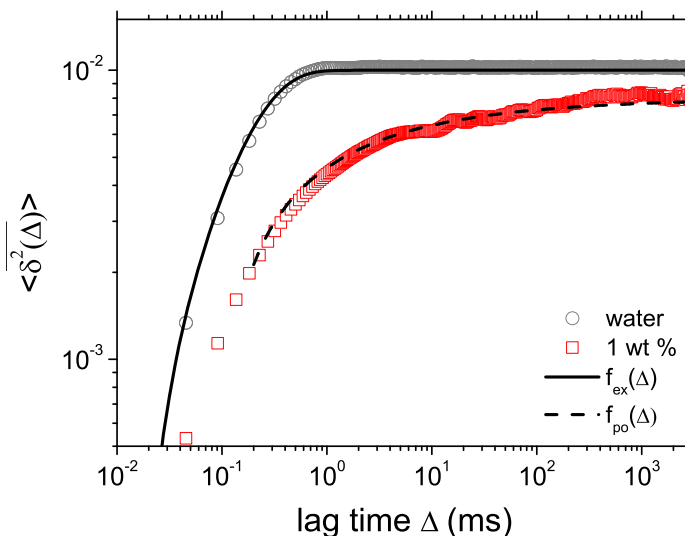
Figure 2. Comparison of the TA MSD $\overline{\langle \delta^2(\Delta) \rangle}$ from ten individual trajectories for beads of $d = 0.96\,\mu\mathrm{m}$ size, in a 1 wt% worm-like micellar solution compared to the control data in pure water. Two different fitting curves to the results are depicted: the solid line represents the exponential relaxation pattern $f_{\mathrm{ex}}(\Delta) = 2\langle x^2 \rangle_{\mathrm{th}}(1 - C_1 \mathrm{e}^{-C_2\Delta})$, while the dashed line represents the power-law relaxation behaviour $f_{\mathrm{po}}(\Delta) = 2\langle x^2 \rangle_{\mathrm{th}}(1 - C_3/\Delta^{C_4})$. Using the fit parameters C_i and the diffusion coefficient K_α for the corresponding beads independently determined from the video tracking results shown in figure 4, a rough estimate for the calibration of the length scale in the TA MSD of the optical tweezers measurements may be obtained. For the data shown here the arbitrary units are converted to nm^2 by multiplication with $\approx 8 \times 10^3$.

not adequately describe the slow relaxation for the bead in the worm-like micellar solution. Surprisingly, we find that this slow relaxation is indeed explained by the confined anomalous diffusion behaviour as governed by the FLE (see section 2.3). In this case, the TA MSD follows the power-law (9) towards saturation. As demonstrated in figure 2, the power-law fit function $f_{\mathrm{po}}(\Delta) = 2\langle x^2 \rangle_{\mathrm{th}}(1 - C_3/\Delta^{C_4})$ quantitatively describes the long-time relaxation profile for the bead in the micellar solution remarkably well. Note that in the relaxation curve (9), the confinement effect due to the stiffness k only enters into the prefactor of the power-law correction, and the scaling exponent α exclusively determines the relaxation dynamics. From the best fit we obtain $\alpha \approx 0.34(\pm 0.04)$ for beads of size $d = 0.96\,\mu\mathrm{m}$ (where the uncertainty indicates the standard deviation from the fit values to ten individual TA MSD curves). This confirms that at millisecond times the beads have FLE-like anomalous diffusion with the anomalous diffusion exponent $\alpha \approx 0.34(\pm 0.04)$.

In figure 1, larger beads of diameter $d = 2.5\,\mu\mathrm{m}$ seemingly display an extremely long relaxation, even compared to the dynamics of the $0.96\,\mu\mathrm{m}$ beads studied in figure 2. Within our observation time window, the TA MSDs appear to show a second power-law scaling with an apparent exponent 0.28 after the crossover, without ever approaching a plateau. This behaviour could be reminiscent of the weak ergodicity breaking that emerges in the confined CTRW motion [53] (see section 2.3), as previously observed for endogenous lipid granules in living
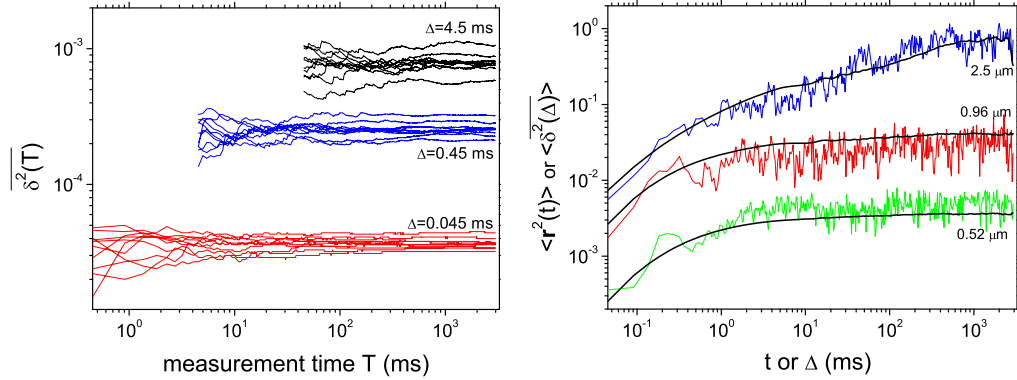
Figure 3. Left: TA MSDs $\overline{\delta^2(T)}$ as a function of the measurement time T at given lag times $\Delta = 0.045$, 0.45 and 4.5 ms. No significant dependence on T is detected, showing that the observed process does not age. Right: comparison of the EA MSD $\langle \mathbf{r}^2(t) \rangle$ (coloured thin lines) and the TA MSD $\langle \overline{\delta^2(\Delta)} \rangle$ (black thick lines) from the ten trajectories for each bead size shown in figure 1.

cells [15, 56]. We check in our micellar system the possibility of weak ergodicity breaking for the largest beads by investigating the ageing properties of the TA MSDs. Figure 3 depicts $\overline{\delta^2(\Delta, T)}$ as a function of the measurement time T at given lag times $\Delta = 0.045$, 0.45 and 4.5 ms. In all cases the TA MSDs have essentially no dependence on T, suggesting that the diffusion in the worm-like micelles is ergodic. Consistent conclusions are also deduced from figure 3 (right), where the conventional EA MSDs $\langle \mathbf{r}^2(t) \rangle$ are presented with the averaged TA MSDs $\langle \overline{\delta^2(\Delta)} \rangle$ with the identification $t \leftrightarrow \Delta$. Although the EA MSDs exhibit fluctuations in their profiles due to insufficient statistics of the finite time series, both quantities reasonably agree with each other. For the case of the largest bead, in particular, the EA MSD continuously increases with time in the same manner as the TA MSD $\langle \overline{\delta^2(\Delta)} \rangle$. If the motion were of the non-ergodic CTRW kind, the EA MSD would saturate and thus show strong disagreement with the TA MSD. In fact, we speculate that the power-law scaling after $\sim$1 ms shown in the TA MSD of the 2.5 μm bead reflects their free subdiffusive motion under weak confinement by the optical trapping in the case when the diameter of the bead is significantly larger than the wavelength of the laser used [61]. Consequently, in this case the TA MSD does not follow the power-law decay to a stationary plateau described by equation (9). This speculation is strongly supported by the fact that the obtained anomaly exponent $\alpha \approx 0.28$ is close to the value $\alpha \approx 0.25$ for their free subdiffusive motion obtained by the video tracking (see the inset of figure 4) on the same timescales. From these observations, for all beads investigated here there is no weak ergodicity breaking, and the diffusion process is best described by the FLE corresponding to anomalous diffusion in a viscoelastic environment.

3.2. Long-time free diffusion measured by video tracking

To obtain insight into the diffusion of the beads in the worm-like micellar solution at longer times, we investigate their motion by video microscopy tracking. Different from the above optical tweezers method, this method provides information on the free diffusive motion of the beads in the solution. We also note that in this case the TA MSD is calibrated, and we see that
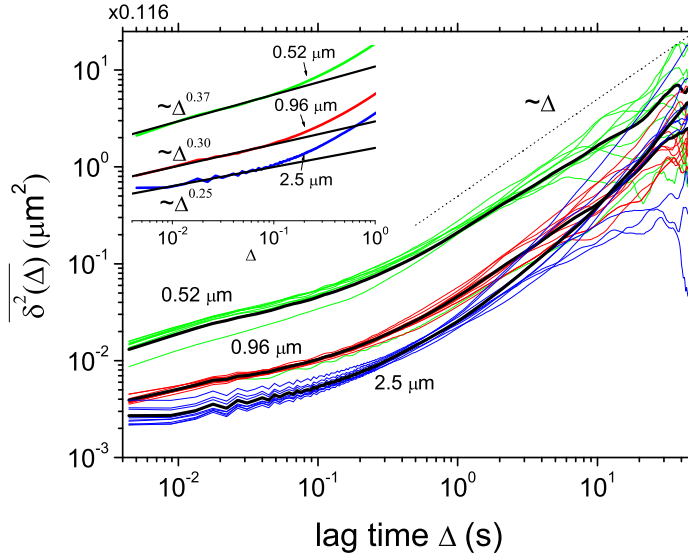
Figure 4. TA MSD curves $\overline{\delta^2(\Delta)}$ for, respectively, ten beads of diameters $d = 0.52\,\mu$m (green), $0.96\,\mu$m (red) and $2.5\,\mu$m (blue) as monitored by video tracking in a 1 wt% worm-like micellar solution. In each case, the thick black line represents the average curve $\langle\overline{\delta^2(\Delta)}\rangle$ from the ten individual TA MSDs. Inset: scaling laws of the averaged TA MSDs $\langle\overline{\delta^2(\Delta)}\rangle$ on sub-second timescales at which subdiffusive motion is observed. Best fits using $f_{\mathrm{fr}}(\Delta) = 4K_\alpha\Delta^\alpha$ are shown in black solid lines with the estimated subdiffusion exponents and generalized diffusion coefficients: $\alpha \approx 0.37(\pm0.05)$ and $K_\alpha \approx 3.1(\pm0.9) \times 10^{-3}$ (μm^2 s$^{-\alpha}$) (bead size $0.52\,\mu$m); $\alpha \approx 0.30(\pm0.02)$ and $K_\alpha \approx 5.8(\pm0.3) \times 10^{-4}$ (μm^2 s$^{-\alpha}$) (bead size $0.96\,\mu$m); and $\alpha \approx 0.25(\pm0.03)$ and $K_\alpha \approx 2.7(\pm0.2) \times 10^{-4}$ (μm^2 s$^{-\alpha}$) (bead size $2.5\,\mu$m).

(at least, initially) the largest bead has the smallest MSD, as it should. Figure 4 presents the TA MSD curves from 10 trajectories for beads of diameters $d = 0.52$, 0.96 and $2.5\,\mu$m, along with their average curve $\langle\overline{\delta^2(\Delta)}\rangle$ (thick black lines). It is shown that the long-time motion of the individual beads is again homogeneous in the sense that the TA MSD curves for same-sized beads exhibit consistent behaviour. In figure 4, all trajectories for all bead sizes display qualitatively consistent diffusive motions with only small amplitude scatter around the average behaviour. Only at longer times do the trajectories split up pronouncedly, including a strong variation of slopes.

More specifically, on sub-second timescales ($\lesssim 1$ s), the diffusion is subdiffusive, $\overline{\delta^2(\Delta)} \sim \Delta^\alpha$ with $0 < \alpha < 1$. As shown in figure 4 (inset), we estimate the subdiffusion exponent α of the diffusion at sub-second times for the three bead sizes by fitting of the power-law behaviour $\langle\overline{\delta^2(\Delta)}\rangle$ with the form of the free diffusion $f_{\mathrm{fr}}(\Delta) = 4K_\alpha\Delta^\alpha$. The estimated values of the anomalous diffusion exponent are clearly below unity, and they tend to decrease with increasing bead size, as expected. Note that the subdiffusion in the video tracking data overlaps with the time scales at which the slow algebraic relaxation described by equation (9) appears, as discussed in the previous subsection. For beads of size $0.96\,\mu$m, the anomalous diffusion exponent $\alpha \approx 0.34$ obtained from the relaxation profile with the help of equation (9) is in good
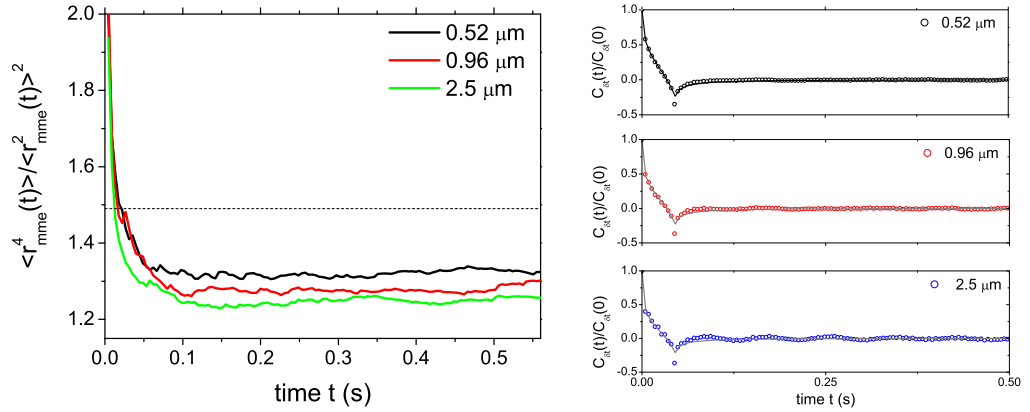
Figure 5. (Left) The moment ratio $\langle r_{\mathrm{mme}}^4(t)\rangle/\langle r_{\mathrm{mme}}^2(t)\rangle^2$ of the mean maximal excursion for the video-tracked beads presented in figure 4. Here $r_{\mathrm{mme}}(t)$ is the maximal 2D distance up to time t, travelled by a given bead, from its initial position. The dotted line (1.49) represents the critical value distinguishing the subdiffusive CTRW from the subdiffusive FLE motion: the former/latter attains the ratio above/below this value. (Right) The normalized velocity autocorrelation function $C_{\delta t}(t)/C_{\delta t}(0)$ for the three different sized beads, along with the theoretical curve according to FLE. The velocity of a bead was defined in an average sense to $\mathbf{v}(t) = [\mathbf{r}(t+\delta t) - \mathbf{r}(t)]/\delta t$ with $\delta t = 10$ frame-intervals ≈ 0.044 (s), and the velocity autocorrelation was then obtained as $C_{\delta t}(t) = \langle \mathbf{v}(t)\mathbf{v}(0)\rangle$. The solid line shows $C_{\delta t}(t)/C_{\delta t}(0) = [(t+\delta)^\alpha - 2t^\alpha + (t-\delta)^\alpha]/(2\delta t^\alpha)$ for FLE motion with α given by the value obtained from the fitting in figure 4.

agreement with the value $\alpha \approx 0.30$ fitted to the video tracking data. Note, however, that while here the exponent α is obtained from a straight-line fit to the TA MSD in figure 4, in the optical tweezers measurement of figures 1 and 2 the value for α is found through fit to equation (9).

To cross-check that this (free) subdiffusive motion is also governed by the fractional Langevin equation, we performed additional tests. In figure 5 (left), we analysed the moment ratio $\langle r_{\mathrm{mme}}^4(t)\rangle/\langle r_{\mathrm{mme}}^2(t)\rangle^2$ of the mean maximal excursion for the motions. For all beads, the ratios are below the critical value (dotted line), indicating that their subdiffusive motions belong to FLE motion. In figure 5 (right), we compared the normalized velocity autocorrelation function $C_{\delta t}(t)/C_{\delta t}(0)$ for the beads to the theoretical prediction by FLE (solid line). The velocities of the beads show the expected anti-correlation in reasonable agreement with the prediction of FLE motion. From these analyses, we conclude that the ergodic anomalous diffusion governed by FLE consistently explains the confined as well as the free diffusive motion studied by optical tweezers and video tracking. We note that while the distribution of the amplitude scatter of the TA MSD around its trajectory-to-trajectory ensemble average in principle allows one to distinguish different stochastic processes from each other (see, for instance, [40, 62]), the statistics from the relatively few trajectories recorded here does not allow a clear distinction between different stochastic processes.

At longer times ($\Delta \gtrsim 1\,\mathrm{s}$) the behaviour of the diffusion changes significantly. In the majority of trajectories the diffusion becomes almost normal, $\alpha \approx 1$. However, especially in the case of the largest beads, we see distinct superdiffusive behaviour with α assuming values

above 1, albeit not for all of the trajectories. The observed superdiffusion persists up to the end of the measured time window, and the largest beads even become absolutely faster than the smallest beads.

4. Discussion

In this work, we investigated the diffusive behaviour of micron-sized beads immersed in aqueous solutions of worm-like micelles based on single-trajectory analyses using optical tweezers and video tracking setups. Our motivation is to obtain insight into the diffusion in complex fluids, in particular, crowded media. To perform experiments in controllable artificial environments is vital towards understanding the even more complex environment inside living biological cells. While we here obtain results at shorter times that are consistent with the motion in viscoelastic media, the bivariate behaviour (normal versus superdiffusion) at longer times to our knowledge has not been observed in this context.

At very short times (sub-millisecond) the observed beads perform normal Brownian diffusion. This could simply mean that the motion of the beads in the relatively low micelle concentration of 1 wt% is not yet hindered and corresponds to the motion in a simple liquid. On the range of milliseconds the motion turns anomalous, with subdiffusion exponents of the order of $\alpha \approx 0.3$ for all observed beads. This subdiffusion was shown to be consistently described with the motion in a viscoelastic environment as described by the FLE. Finally, at around 1 s the motion accelerates and becomes Brownian or even superdiffusive. The latter occurs mainly for the largest beads.

In early studies based on diffusing wave spectroscopy [30, 31], diffusion in worm-like micellar solutions was interpreted such that the micron-sized beads perform confined Brownian motion on time scales from sub-milliseconds to milliseconds (as described by the form (4)). After entrapment in their 'cage', at longer times in the second range the stuck beads again perform Brownian motion, such that the worm-like micelle system behaves like a simple liquid. Based on this interpretation, the obtained EA MSD curve was described by the functional form

$$\langle \mathbf{r}^2(t) \rangle = 6R^2(1 - e^{-(K_0 t/R^2)^\beta})^{1/\beta} \left(1 + \frac{K_m}{R^2} t \right) \tag{10}$$

where K_0 and K_m are, respectively, the microscopic (short-time) and macroscopic (long-time) diffusion constants of the beads, and R is the effective size of the cage. In this expression, the additional fitting exponent β was introduced to account for the subdiffusive scaling in the intermediate time scale, which is not explained within the scheme of ordinary Brownian motion.

However, our study based on single-particle tracking experiments convincingly shows that such simple corralled Brownian motion is not an appropriate scenario for the observed diffusion. On time scales at which the system is viscoelastic, the diffusion should rather be understood as anomalous diffusion governed by the FLE. This is highlighted in the relaxation dynamics of the beads trapped by optical tweezers. For beads immersed in the worm-like micellar solution, the relaxation curve shows a distinct power-law-like decay lasting over several decades in time, as predicted previously for confined FLE motion [32]. This slow, anomalous relaxation partially overlaps with the measured free anomalous diffusion in the video tracking experiments. We note that while we identify FLE as the best known stochastic model for bead motion on the observed time scales, it cannot explain the free Brownian motion of beads at shorter times and the coupled Brownian motion of beads and micelles at longer times. A complete model will

incorporate these two regimes and the respective turnovers. However, such a model is not within the scope of this study.

Importantly, our experiments suggest that the viscoelastic property of the media indeed leads to FLE-like anomalous diffusion for the embedded particle, characterized by algebraically decaying spatial correlations of random displacements and ergodicity. Although there are some clues that the FLE-like anomalous diffusion is closely connected to the viscoelasticity [13, 22], to the best of our knowledge, a systematic study is presented here for the first time showing experimental evidence for the power-law relaxation dynamics of the TA MSD. Thus, while free anomalous motion governed by the FLE is ergodic and $\langle \mathbf{r}^2(\Delta) \rangle = \langle \overline{\delta^2(\Delta)} \rangle$, when the test particle engages with the confinement this equivalence is (transiently) broken. This has profound consequences for the interpretation of the dynamic relaxation in the presence of confinement and the related time scale(s).

What can we say about the occurrence of normal and superdiffusive motion at longer times? While at the moment we do not have conclusive evidence, we may speculate that the smaller beads experience a regular liquid-like environment, in which they exhibit normal diffusion. This could indeed be related to the depolymerization/polymerization of the micelle aggregates. If on average the micelle aggregates rearrange such that there are sufficiently large holes, the smaller beads may be able to move more isotropically and homogeneously, similar to smaller beads in cross-linked actin meshes [63]. The superdiffusion of larger beads may be closely related to the self-recombination of worm-like micelles in the diffusion-controlled regime, during which fragmented worm-like micelles tend to recombine with their original partners [33, 64, 65]. The induced longitudinal stress may lead to the superdiffusion of a bead beyond a certain size when it has no way to escape from its cage and thus moves along with the recombining micelles. However, this effect clearly needs more detailed investigation. We note that for superdiffusive processes, finite *T*-effects may cause a wide spread of the apparent slopes of the TA MSD [66]. This observation may indicate that a significant fraction of the trajectories of larger beads are indeed superdiffusive.

What can we learn with respect to the diffusion of intracellular particles in living cells from our experiments? We saw previously with the same experimental tools that *in vivo* anomalous diffusion of lipid granules in fission yeast [15] and human cells [56] shows CTRW-like motion characterized by weak ergodicity breaking. These granules are of a size comparable to the polystyrene beads used here. Due to the complexity of intracellular environments, it is challenging to deduce the origin of weak ergodicity breaking. Our present study suggests that the viscoelasticity of the cytoplasmic fluid alone may not be sufficient to explain the observed motion, and that either molecular shapes, physical properties specific to the crowding environment, or even various nonspecific interactions may well play a crucial role. Also, previous investigations [67] have shown that the cellular metabolism exerts a major influence on transport mechanisms inside living cells. Hence, the absence of metabolism in *in vitro* networks may explain certain differences in the anomalous diffusion observed between *in vitro* and *in vivo* systems.

Finally, we note that our approach using complementary measurement methods provides a significant advantage. While conventional video tracking delivers information about the free motion over quite a large time window, optical tweezers tracking allows access to shorter time scales and finer spatial resolution. At the same time we also obtain additional information. As shown here the relaxation dynamics to the thermal value of the MSD delivers significant information, in the present case allowing us to decide in favour of the FLE dynamics of viscoelastic diffusion from the observed power-law relaxation.

IOP Institute of Physics ⟐ DEUTSCHE PHYSIKALISCHE GESELLSCHAFT

Acknowledgments

References

[1] Brown R 1828 *Phil. Mag.* **4** 161
[2] Perrin J 1909 *Ann. Chim. Phys.* **18** 1
[3] Nordlund I 1914 *Z. Phys. Chem.* **87** 40
[4] Bräuchle C, Lamb D and Michaelis J 2010 *Single Particle Tracking and Single Molecule Energy Transfer* (Weinheim: Wiley-VCH)
[5] Xie X S, Choi P J, Li G-W, Lee N K and Lia G 2008 *Ann. Rev. Biophys.* **37** 417
[6] Zimmermann S B and Trach S O 1991 *J. Mol. Biol.* **222** 599
[7] Ellis R J and Minton A P 2003 *Nature* **425** 27
[8] McGuffee S R and Elcock A H 2010 *PLoS Comput. Biol.* **6** e1000694
[9] Bouchaud J-P and Georges A 1990 *Phys. Rep.* **195** 127
[10] Metzler R and Klafter J 2000 *Phys. Rep.* **339** 1
[11] Metzler R and Klafter J 2004 *J. Phys. A: Math. Gen.* **37** R161
[12] Golding I and Cox E C 2006 *Phys. Rev. Lett.* **96** 098102
[13] Weber S, Spakowitz A J and Theriot J A 2010 *Phys. Rev. Lett.* **104** 238102
[14] Caspi A, Granek R and Elbaum M 2000 *Phys. Rev. Lett.* **85** 5655
[15] Jeon J-H, Tejedor V, Burov S, Barkai E, Selhuber-Unkel C, Berg-Sørensen K, Oddershede L and Metzler R 2011 *Phys. Rev. Lett.* **106** 048103
[16] Seisenberger G, Ried M U, Endreß T, Büning H, Hallek M and Bräuchle C 2001 *Science* **294** 1929
[17] Bronstein I, Israel Y, Kepten E, Mai S, Shav-Tal Y, Barkai E and Garini Y 2009 *Phys. Rev. Lett.* **103** 018102
[18] Weiss M, Elsner M, Kartberg F and Nilsson T 2004 *Biophys. J.* **87** 3518
[19] Vercamman J, Martens G and Engelborghs Y 2007 *Springer Ser. Fluoresc.* **4** 323
[20] Banks D and Fradin C 2005 *Biophys. J.* **89** 2960
[21] Pan W, Fibelo L, Pham N D Q, Galin O, Uzunova V V and Vekilov P G 2009 *Phys. Rev. Lett.* **102** 058101
[22] Szymanski J and Weiss M 2009 *Phys. Rev. Lett.* **103** 038102
[23] Weiss M, Hashimoto H and Nilsson T 2003 *Biophys. J.* **84** 4043
[24] Weigel A V, Simon B, Tamkun M M and Krapf D 2011 *Proc. Natl Acad. Sci. USA* **108** 6438
[25] Kneller G R, Baczynski K and Pasenkiewicz-Gierula M 2011 *J. Chem. Phys.* **135** 141105
[26] Akimoto T, Yamamoto E, Yasuoja K, Hirano Y and Yasui M 2011 *Phys. Rev. Lett.* **107** 178103
[27] Jeon J-H, Martinez-Seara Monne H, Javanainen M and Metzler R 2012 *Phys. Rev. Lett.* **109** 188103
[28] Javanainen M, Hammaren H, Monticelli L, Jeon J-H, Metzler R and Vattulainen I 2013 *Faraday Discuss.* **161** 397
[29] Dreiss C A 2007 *Soft Matter* **3** 956
[30] Galvan-Miyoshi J, Delgado J and Castillo R 2008 *Eur. Phys. J.* E **26** 369
[31] Bellour M, Skouri M, Munch J-P and Hébraud P 2002 *Eur. Phys. J.* E **8** 431
[32] Jeon J-H and Metzler R 2012 *Phys. Rev.* E **85** 021147
[33] Ott A, Bouchaud J-P, Langevin D and Urbakh W 1990 *Phys. Rev. Lett.* **65** 2201
[34] Buchanan M, Atakhorrami M, Palierne J F and Schmidt C F 2005 *Macromolecules* **38** 8840
[35] Peterman E, Gittes F and Schmidt C F 2003 *Biophys. J.* **84** 1308
[36] Bendix P M, Reihani S N S and Oddershede L B 2010 *ACS Nano* **4** 2256
[37] Richardson A C, Reihani S N S and Oddershede L B 2008 *Opt. Express* **16** 15709
[38] Sbalzarini I F and Koumoutsakos P 2005 *J. Struct. Biol.* **151** 182

[39] Barkai E, Garini Y and Metzler R 2012 *Phys. Today* **65** 29
[40] Burov S, Jeon J-H, Metzler R and Barkai E 2011 *Phys. Chem. Chem. Phys.* **13** 1800
[41] Deng W and Barkai E 2009 *Phys. Rev.* E **79** 011112
[42] Jeon J-H and Metzler R 2010 *Phys. Rev.* E **81** 021103
[43] Montroll E W and Weiss G H 1965 *J. Math. Phys.* **6** 167
[44] Scher H and Montroll E W 1975 *Phys. Rev.* B **12** 2455
[45] Lubelski A, Sokolov I M and Klafter J 2008 *Phys. Rev. Lett.* **100** 250602
[46] He Y, Burov S, Metzler R and Barkai E 2008 *Phys. Rev. Lett.* **101** 058101
[47] Sokolov I M, Heinsalu E, Hänggi P and Goychuk I 2009 *Europhys. Lett.* **86** 30009
[48] Boyer D, Dean D S, Mejía-Monasterio C and Oshanin G 2012 *Phys. Rev.* E **85** 031136
[49] Bouchaud J-P 1992 *J. Phys.* I **2** 1705
[50] Bel G and Barkai E 2005 *Phys. Rev. Lett.* **94** 240602
[51] Rebenshtok A and Barkai E 2007 *Phys. Rev. Lett.* **99** 210601
[52] Lomholt M A, Zaid I M and Metzler R 2007 *Phys. Rev. Lett.* **98** 200603
[53] Burov S, Metzler R and Barkai E 2010 *Proc. Natl Acad. Sci. USA* **107** 13228
[54] Tejedor V, Bénichou O, Voituriez R, Jungmann R, Simmel F, Selhuber-Unkel C, Oddershede L and Metzler R 2010 *Biophys. J.* **98** 1364
[55] Magdziarz M, Weron A, Burnecki K and Klafter J 2009 *Phys. Rev. Lett.* **103** 180602
[56] Leijnse N, Jeon J-H, Loft S, Metzler R and Oddershede LB 2012 *Eur. Phys. J. Spec. Top.* **204** 75
[57] Schulz J H P, Barkai E and Metzler R 2013 *Phys. Rev. Lett.* **110** 020602
[58] Lutz E 2001 *Phys. Rev.* E **64** 051106
[59] Goychuk I 2009 *Phys. Rev.* E **80** 046125
[60] Sokolov I M 2012 *Soft Matter* **8** 9043
[61] Rohrbach A 2005 *Phys. Rev. Lett.* **95** 168102
[62] Jeon J H and Metzler R 2010 *J. Phys.* A **43** 252001
[63] Wong I Y, Gardel M L, Reichman D R, Weeks E R, Valentine M T, Bausch A R and Weitz D A 2004 *Phys. Rev. Lett.* **92** 178101
[64] Ganapathy R, Sood A K and Ramaswamy S 2007 *Europhys. Lett.* **77** 18007
[65] Angelico R, Ceglie A, Olsson U, Palazzo G and Ambrosone L 2006 *Phys. Rev.* E **74** 031403
[66] Godec A and Metzler R 2013 *Phys. Rev. Lett.* **110** 020603
[67] Winther T, Xu L, Berg-Sørensen K, Brown S and Oddershede LB 2009 *Biophys. J.* **97** 1